Dispersion of bamboo type multi-wall carbon nanotubes in calf-thymus double stranded DNA

Emiliano N. Primo [a], Paulina Cañete-Rosales [b], Soledad Bollo [b], María D. Rubianes [a,*], Gustavo A. Rivas [a,*]

[a] INFIQC, Departamento de Físico Química, Facultad de Ciencias Químicas, Universidad Nacional de Córdoba, Ciudad Universitaria, 5000 Córdoba, Argentina
[b] Facultad de Ciencias Químicas y Farmacéuticas, Universidad de Chile, Santiago, Chile

ARTICLE INFO

ABSTRACT

We report for the first time the use of double stranded calf-thymus DNA (dsDNA) to successfully disperse bamboo-like multi-walled carbon nanotubes (bCNT). The dispersion and the modified electrodes were studied by different spectroscopic, microscopic and electrochemical techniques. The drastic treatment for dispersing the bCNT (45 min sonication in a 50% (v/v) ethanol:water solution), produces a partial denaturation and a decrease in the length of dsDNA that facilitates the dispersion of CNT and makes possible an efficient electron transfer of guanine residues to the electrode. A critical analysis of the influence of different experimental conditions on the efficiency of the dispersion and on the performance of glassy carbon electrodes (GCE) modified with bCNT–dsDNA dispersion is also reported. The electron transfer of redox probes and guanine residues was more efficient at GCE modified with bCNT dispersed in dsDNA than at GCE modified with hollow CNT (hCNT) dispersed in dsDNA, demonstrating the importance of the presence of bCNT.

1. Introduction

The unique properties of nanomaterials have placed them in the forefront of emerging technologies and have made possible the unprecedented growth of the nanosciences field in the last decade. Carbon nanotubes (CNT) represent a very exciting group of nanomaterials due to their amazing properties connected with their particular structure, high thermal and chemical stability, and excellent conductivity [1].

CNT are one of the allotropes of carbon and consist of carbon atoms with sp^2 hybridization arranged in graphene sheets rolled up in a tube [1–3]. According to the number of rolled-up sheets, they can be classified in single-wall (SWCNT) and multi-wall CNT (MWCNT) [3–5]. The latter ones have a veriety of structures depending on the presence of side-defects, the hollow ones (hCNT) have ideally defect-free side walls while the bamboo-like ones (bCNT) present transverse walls regularly located along the tubes resulting in edge planes of graphene material at regular intervals along the walls [6].

Gooding et al. [7] reported an important improvement in the voltammetric response of $[Fe(CN)_6]^{3-}$ as well as a significant enhancement in the sensitivity for the electrooxidation of single-stranded calf-thymus DNA at glassy carbon electrodes (GCE) modified with bCNT dispersed in ethanol. Gedanken and Shanmugam [8,9] demonstrated that the electrodes modified with bCNT present a faster electron transfer compared to those containing hCNT due to a better wettability and the presence of edge-plane-like defects and oxygenated functional groups.

Due to the poor solubility of CNT in water and common organic solvents they must be previously functionalized for developing electrochemical sensors [10]. This functionalization involves both covalent and non-covalent interactions [11–13]. The covalent approach is usually performed after a drastic oxidation step that generates oxygenated functions on the CNT. Even when this functionalization has demonstrated to be very useful for different applications [14], it produces changes in the electronic properties [11–13]. The non-covalent functionalization has received great attention in the last years since it allows a successful derivatization of CNT without disturbing their unique electronic characteristics [13]. One of the strategies to achieve this functionalization is the preparation of dispersions of CNT in different media. Ultrasonication plays an important role in debundling and dispersing the nanotubes. The driving force comes from the cavitation, which involves a process of bubble formation, growth and collapse [15]. Chen et al. [16] demonstrated that the parameters associated with the sonication process, rather than solvent solubility parameters, govern the dispersion process.

* Corresponding authors. Tel.: +54 351 4334169/80; fax: +54 351 4334188.
E-mail addresses: rubianes@fcq.unc.edu.ar (M.D. Rubianes),
grivas@fcq.unc.edu.ar, rivasgus@yahoo.com.ar (G.A. Rivas).

Surfactants, biomolecules and polymers have been successfully used to disperse CNT [17]. These molecules not only disperse the CNT but also give to them particular properties associated with the nature of the polymer. CNT are wrapped by polymers forming supramolecular complexes mainly by π-stacking with CNT surface [18]. Nafion [19,20], chitosan [21], polyethylenimine [22–25], polylysine [26,27], polydiallyldimethyl ammonium (PDDA) [28], polyacrylic acid [29,30], hialuronic acid [31], ionic-liquids [32], lysozyme [33], glucose oxidase [34], surfactants [35] and polyhistidine [36], have been successfully used as dispersing agents.

Sperm salmon double stranded DNA (dsDNA) [37] and oligonucleotides [38,39] have been used to prepare CNT dispersions. In general, most of the results have been obtained using SWCNT, although in some cases MWCNT have been also employed. Li et al. [40] reported the effective dispersion of MWCNT in aqueous single stranded DNA (ssDNA) solution by sonication. They proposed that ssDNA interacts with CNT walls by adsorption of the nitrogen bases during the ultrasonic treatment through π–π stacking, leaving the sugar-phosphate backbone exposed to the solution. Karachevtsev et al. [38] described the adsorption of poly(rA) on the CNT surface through π–π stacking between the nanotubes and adenine residues. Molecular dynamics simulations demonstrated that more than half of the adenine residues are not stacked on CNT walls and that some of them undergo self-stacking. Wallace et al. [37] stated that the sonication of SWCNT with salmon sperm DNA and other biopolymers produces stable isotropic dispersions. Spectroscopic experiments and DFT calculations demonstrated that the sidewalls defects of CNT are effective for dispersing CNT in aqueous DNA solutions [41]. Hughes et al. [42] compared the dispersing properties of different homo-oligonucleotides and found that the one containing only thymine was the most efficient for dispersing SWCNT, although the fastest dispersion was obtained with the oligonucleotides containing only cytosine.

Here, we report for the first time the use of calf-thymus dsDNA to efficiently disperse bCNT. In the following sections we discuss the advantages of using bCNT instead of hCNT, the influence of different experimental conditions (sonication time, solvent, bCNT:dsDNA ratio) on the efficiency of the dispersion and on the performance of GCE modified with bCNT–dsDNA dispersion. Different spectroscopic and electrochemical techniques and high-resolution microscopy have been used for studying the system.

2. Experimental

2.1. Apparatus

The amperometry and cyclic voltammetry measurements were performed with EPSILON (BAS) and Autolab (PGSTAT 128N Eco-Chemie) potentiostats. The electrodes were inserted into the cell through holes in its Teflon cover. A platinum wire and Ag/AgCl, 3 M NaCl (BAS) were used as counter and reference electrodes, respectively. All potentials are referred to the latter. A magnetic stirrer provided the convective transport during the amperometric measurements.

Scanning electronic microscopy (SEM) images were obtained with a Hitachi S3000N Microscope equipped with secondary and back-scattered electron detectors. Transmission electronic microscopy (TEM) was done with a JEOL-2000 FXII electron microscope operated at 200 KeV.

Electrochemical impedance spectroscopy (EIS) measurements were performed with a Solartron 1287 FRA 1260. UV–vis experiments were carried out with a Shimadzu UV1700 Pharma spectrometer. Fourier Transform Infrared Spectroscopy (FTIR) spectra were obtained with a Nicolet 5-SX C spectrometer. For scanning electrochemical microscopy (SECM) measurements, a ∼10 μm

diameter home-made carbon fiber electrode served as SECM tip, while glassy carbon electrodes (GCE) of 3 mm diameter (Model CHI104, CH Instruments) were used as SECM substrates.

2.2. Reagents

Hydrogen peroxide (H_2O_2, 30% (v/v) aqueous solution) was purchased from Baker. Ferrocene methanol (FcOH) and calf-thymus double stranded DNA (dsDNA, Catalog number D 4522) were purchased from Sigma. Potassium ferrocyanide and potassium ferricyanide were obtained from Merck. Bamboo-like multiwalled carbon nanotubes (bCNT, diameter (30 ± 10) nm, length 1–5 μm, 98.92% purity) and hollow-type multiwalled carbon nanotubes (hCNT, diameter (30 ± 15) nm, length 1–5 μm, 98.92% purity) were obtained from NanoLab (U.S.A.). The CNT powders were used pristine and no chemical purification or further activation was performed. Other chemicals were of reagent grade and were used without further purification. Ultrapure water ($\rho = 18.2$ MΩ cm) from a Millipore-MilliQ system was used for preparing all the solutions. A 0.200 M acetate buffer solution pH 5.00 and 0.050 M phosphate buffer solution pH 7.40 were used as supporting electrolytes.

2.3. Preparation of modified GCE

2.3.1. Pretreatment of GCE
Before modification, the GCE were polished with alumina slurries of 1.0, 0.3 and 0.05 μm for 1.5 min each and then electrochemically pretreated by performing cyclic voltammograms between −0.300 and 0.700 V in a 0.050 M phosphate buffer solution pH 7.40 at a scan rate of 0.100 V s^{-1} (10 cycles). After that, the electrodes were carefully dried under a N_2 stream.

2.3.2. Preparation of the dispersions
(a) *bCNT in ethanol/water:* the dispersion was obtained by mixing 1.00 mg of bCNT powder with 1.00 mL of a 50% (v/v) ethanol:water solution followed by sonication for 45 min.
(b) *bCNT in dsDNA (bCNT–dsDNA):* the dispersion was obtained by mixing 1.00 mg of bCNT powder with 1.00 mL of a 100 ppm dsDNA solution (prepared in 50% (v/v) ethanol:water) followed by sonication for 45 min.

For comparison, a dispersion of hCNT in dsDNA was prepared in the same way as bCNT–dsDNA. The solution of dsDNA used to modify the GCE was prepared by sonicating for 15 min a 100 ppm dsDNA solution in 50% (v/v) ethanol:water.

2.3.3. Modification of GCE with bCNT–dsDNA (GCE/bCNT–dsDNA)
The GCE were modified by dropping 20 μL of the bCNT–dsDNA dispersion on the top of the surfaces followed by the evaporation of the solvent by exposure to air for 90 min. A similar protocol was employed to prepare GCE/bCNT, GCE/hCNT–dsDNA and GCE/dsDNA by using dsDNA or the corresponding CNT dispersion.

2.4. Procedure

The amperometric experiments were carried out by applying the desired potential and allowing the transient current to decay to a steady-state value prior to the addition of the analyte and the subsequent current monitoring. All the experiments were conducted at room temperature.

EIS experiments were performed by applying a sinusoidal potential perturbation of 10 mV of amplitude in the frequency range of 10^5–10^{-1} Hz and a working potential corresponding to the formal potential of a 2.0×10^{-3} M [Fe(CN)$_6$]$^{3-/4-}$ solution
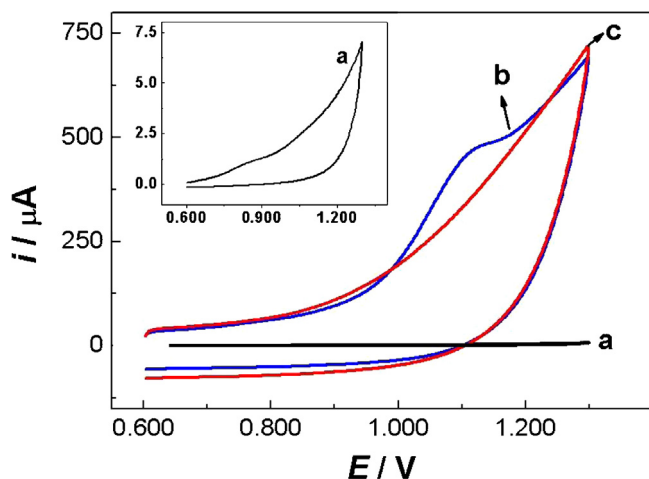
Fig. 1. Cyclic voltammograms obtained at GCE modified with (a) dsDNA (100 ppm), (b) bCNT (1.00 mg mL^{-1})–dsDNA (100 ppm) dispersion and (c) bCNT (1.00 mg mL^{-1}) dispersion; v = 0.100 V s^{-1}. Supporting electrolyte: 0.200 M acetate buffer solution pH 5.00. The inset shows the voltammogram (a) with a larger scale.

($\sim$0.200 V). The impedance spectra were analyzed and fitted by using the Z-view program.

The samples for FTIR experiments were obtained by dropping the dsDNA solution or the CNT-dispersion on a ZnSe disk, followed by the evaporation of the solvent.

SECM experiments were performed using the feedback mode. They were carried out in a 0.100 M phosphate buffer solution pH 7.40 using 5.0×10^{-4} M FcOH as redox mediator. The tip potential was held at 0.500 V to produce the oxidation of FcOH, while the potential of the bare or modified GCE (called substrate) was kept at 0.000 V to allow the feedback between the electrodes (more details about SECM in Supplementary Information).

The results presented here were obtained using three different dispersions and three electrodes in each case.

3. Results and discussion

3.1. GCE/bCNT–dsDNA versus GCE/hCNT–dsDNA

3.1.1. Intrinsic electrochemical response of GCE/bCNT–dsDNA

Fig. 1 displays cyclic voltammograms obtained at 0.100 V s^{-1} in a 0.200 M acetate buffer solution pH 5.00 at GCE/dsDNA (a), GCE/bCNT–dsDNA (b) and GCE/bCNT (c). The i–E profile for GCE/dsDNA shows a small peak current at around 0.800 V due to the oxidation of guanine residues [43] (inset in Fig. 1). On the contrary, at GCE/bCNT–dsDNA the peak current for guanine electrooxidation appears at (1.100 ± 0.002) V and it is 99 times higher than that at GCE/dsDNA, indicating that the close proximity of dsDNA to bCNT in the dispersion and the huge increment of the electroactive area make possible a sensitive oxidation of guanine residues. The cyclic voltammogram obtained at GCE/bCNT (c) only exhibits the solvent oxidation at potentials higher than 0.800 V demonstrating that the current peak observed at GCE/bCNT–dsDNA is effectively due to DNA residues oxidation. At GCE/bCNT–dsDNA there is a linear relationship between the oxidation current at the peak potential and the scan rate, as expected for a surface controlled process (Fig. S1 in Supplementary Information). Therefore, the oxidation current of the electroactive residues of dsDNA can be used as an indicator of the efficiency of dsDNA as dispersing agent of bCNT.

Fig. 2A depicts cyclic voltammograms for GCE modified with dispersions of bCNT (a) and hCNT (b) in 100 ppm dsDNA performed in 0.200 M acetate buffer solution pH 5.00. At GCE/bCNT–dsDNA the oxidation peak potential due to the oxidation of guanine residues

is 130 mV lower than that obtained at GCE/hCNT–dsDNA and the associated current is around 30% higher, indicating a facilitated electro-oxidation of dsDNA at GCE/bCNT–dsDNA. These results are in agreement with those reported by Compton et al. [44] who demonstrated that the maximum electrocatalytic activity is reached at edge-plane regions. The inset shows the cyclic voltammograms after baseline correction.

3.1.2. Hydrogen peroxide electrochemical response

Fig. 2B depicts the amperometric profiles at -0.100 V for GCE modified with bCNT–dsDNA (a) and hCNT–dsDNA (b) for successive additions of 1.0×10^{-3} M H$_2$O$_2$. Although the reduction of H$_2$O$_2$ takes place at both electrodes, at GCE/bCNT–dsDNA the signals are better defined and more sensitive. In fact, the sensitivity drastically increases from $(2.8 \pm 0.3) \times 10^3$ μA M^{-1} at GCE/hCNT–dsDNA to $(2.9 \pm 0.1) \times 10^4$ μA M^{-1} at GCE/bCNT–dsDNA. These results clearly demonstrate that the presence of a higher density of edge-like defects at bCNT improves the catalytic activity of the electrode modified with bCNT–dsDNA, in agreement with previous reports [45,46].

3.2. Electrochemical behavior of GCE/bCNT–dsDNA using redox probes

Fig. 3A shows the voltammetric profiles for 2.0×10^{-3} M [Fe(CN)$_6$]$^{3-}$ at bare GCE (a), GCE/bCNT (b), GCE/dsDNA (c), and GCE/bCNT–dsDNA (d). As expected, the voltammogram at bare GCE (a) indicate a quasi-reversible electron transfer process with a peak potential separation (ΔE_p) of (78 ± 2) mV. Upon the modification with bCNT (b), there is an increase of 73% in the current density for the reduction of [Fe(CN)$_6$]$^{3-}$ while ΔE_p diminishes until (61 ± 2) mV. These results demonstrate once again the advantages of the high density of edge-plane like defects present in the bCNT structure, which act as electroactive centers for the electron transfer process. The ΔE_p obtained at GCE/dsDNA (c) is $(5.2 \pm 0.2) \times 10^2$ while the current density decays 46% compared to the bare electrode. These results can be attributed to the electrostatic repulsion between the negatively charged redox probe and the negatively charged phosphate backbone of dsDNA. On the contrary, when the electrode is modified with bCNT–dsDNA dispersion (d) the ΔE_p of the redox couple is reduced to (213 ± 9) mV, demonstrating that, even in the presence of the negatively charged nucleic acid, the electron transfer of the probe improves due to the presence of the edge-plane like defects in bCNT and to a rearrangement of the dsDNA that supports CNT, resulting in a faster electrochemical response.

The electrochemical activity of the different electrodes was also evaluated by EIS. It is known that this technique is a very useful tool to understand the interfacial properties of a given surface with minimal electric perturbation [47]. Fig. 3B depicts Nyquist plots (normalized by the electroactive area of each surface) for GCE (a), GCE/bCNT (b), GCE/dsDNA (c), and GCE/bCNT–dsDNA (d) obtained at 0.200 V in a 2.0×10^{-3} M [Fe(CN)$_6$]$^{3-/4-}$ solution. With exception to GCE/bCNT, the Nyquist profiles for all the platforms show a semicircle at high frequencies (low values of impedance) and a linear increase of the impedance at low frequencies. This behavior can be modeled with a typical Randles circuit [48]. As it is shown in Fig. 3B(b), the resistance associated with the charge transfer (R_{ct}) at GCE/bCNT is very small, in agreement with the low ΔE_p obtained by cyclic voltammetry, indicating that the diffusion controls the overall process in the investigated frequency range (for further details of the circuit used to fit the GCE/bCNT, see supplementary information). Comparing the R_{ct} for GCE, GCE/dsDNA and GCE/bCNT–dsDNA, is clear that the dsDNA present at the electrode surface, either as free molecule or as support of the CNT, behaves as a barrier for the charge transfer of
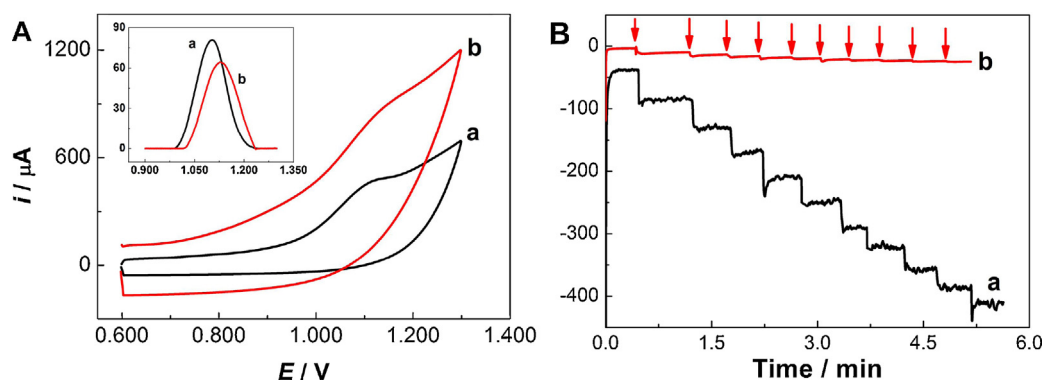
Fig. 2. (A) Cyclic voltammograms obtained at GCE modified with dispersions of (a) 1.00 mg mL^{-1} bCNT–100 ppm dsDNA and (b) 1.00 mg mL^{-1} hCNT–100 ppm dsDNA, both sonicated for 45 min. Supporting electrolyte: 0.200 M acetate buffer solution pH 5.00; $v = 0.100$ V s^{-1}. The inset shows the oxidation peaks with baseline subtraction. (B) Amperometric recordings for successive additions of 1.0×10^{-3} M H$_2$O$_2$ obtained at GCE modified with (a) bCNT (1.00 mg mL^{-1}) and (b) hCNT (1.00 mg mL^{-1}) dispersed in a 100 ppm dsDNA solution. The arrows in (a) indicate the successive additions of H$_2$O$_2$. Working potential: −0.100 V. Supporting electrolyte: 0.050 M phosphate buffer solution pH 7.40.

the redox probe, being this effect more pronounced when GCE is modified just with dsDNA (see more details in Supplementary Information).

By using the R_{ct} the heterogeneous rate constant k^0 of the [Fe(CN)$_6$]$^{3-/4-}$ couple was calculated according to [48]:

$$k^0 = \frac{RT}{n^2 F^2 R_{ct} C_{ox}^{\alpha} C_{red}^{1-\alpha}}$$

where R is the molar gas constant, T is the absolute temperature, n is the number of exchanged electrons, F is the Faraday constant, α is the transfer coefficient and C_{ox} and C_{red} are the bulk concentrations of [Fe(CN)$_6$]$^{3-}$ and [Fe(CN)$_6$]$^{4-}$, respectively. The k^0 values for the redox marker at GCE, GCE/dsDNA and GCE/bCNT–dsDNA were $(2.7 \pm 0.5) \times 10^{-2}$, $(5.1 \pm 0.3) \times 10^{-5}$ and $(3.6 \pm 0.3) \times 10^{-4}$ cm s^{-1}, respectively, correlating the trend obtained for the ΔE_p values previously shown.

In order to evaluate the contribution of the electrostatic interactions and to properly assess the increase of the R_{ct} when comparing GCE with GCE/bCNT–dsDNA platforms, we performed EIS measurements using solutions of different ionic strengths (by adding NaCl solution to the buffer). Table S1 (in Supplementary Information) summarizes the R_{ct} for [Fe(CN)$_6$]$^{3-/4-}$ obtained at GCE, GCE/dsDNA and GCE/bCNT–dsDNA at the different ionic strengths. In all cases, the decrease of R_{ct} with the increase in the ionic strength can be explained by the dependence of the charge transfer rate constant of [Fe(CN)$_6$]$^{3-/4-}$ with the concentration of cations in the solution,

especially when the cation is an alkali metal [49]. This phenomenon is attributed to the formation of an ionic pair between the hexacyanoferrate species and Na$^+$ that reduces the charge of the anionic complex and favors the electron transfer. The drop in the R_{ct} with the increase of the ionic strength observed at GCE/bCNT–dsDNA is higher than that obtained at the bare electrode. Considering that the catalysis of Na$^+$ is a homogeneous process, this additional decrease in the R_{ct} is due to the screening of DNA phosphate backbone charges and the subsequent decrease in the electrostatic repulsion forces between dsDNA and the redox couple. In the case of GCE/dsDNA, the decrease in R_{ct} is less pronounced than at GCE/bCNT–dsDNA indicating that, due to the characteristics of the dsDNA layer, there is a blocking effect not only due to the electrostatic repulsion but also to the nature of physical barrier. In the case of GCE/bCNT, upon rising the salt concentration it was not possible to determine any modification in the interfacial behavior due to the poorly resistive behavior demonstrated for the redox probe within the studied frequency range (more details in Supplementary Information).

The electroactivity of the platform was also evaluated by SECM using FcOH as redox probe. Fig. 4 shows the surface images of GCE (A), GCE/bCNT (B), GCE/dsDNA (C) and GCE/bCNT–dsDNA (D). Compared to GCE, the adsorption of bCNT dispersed in ethanol:water (B) produces an irregular surface indicating that ethanol:water does not disperse efficiently the bCNT. However, the normalized current drastically enhances due to the increase in the electroactive
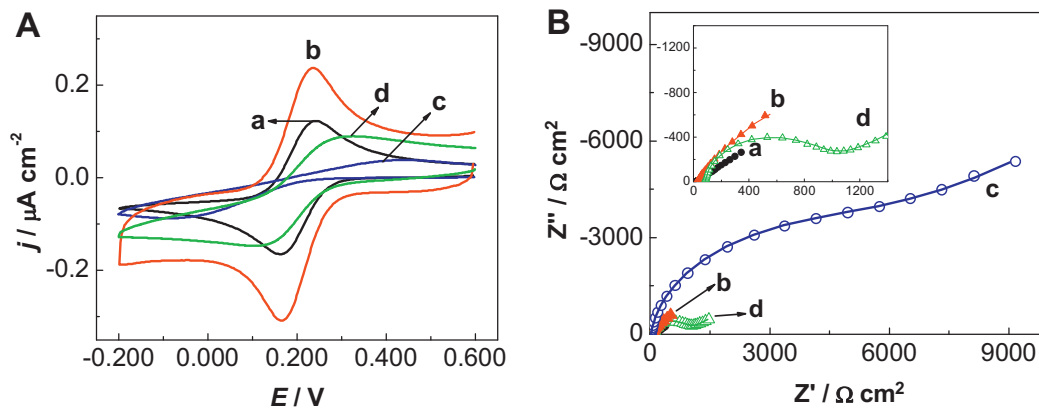

Fig. 3. (A) Cyclic voltammograms obtained at (a) bare GCE, (b) GCE/bCNT, (c) GCE/dsDNA and (d) GCE/bCNT–dsDNA platforms in a 2.0×10^{-3} M [Fe(CN)$_6$]$^{3-}$ solution. Supporting electrolyte: 0.050 M phosphate buffer solution pH 7.40; $v = 0.050$ V s^{-1}. (B) Nyquist plots for impedance spectra obtained for (a, ●) bare GCE, (b, ▲) GCE/bCNT, (c, ○) GCE/dsDNA and (d, △) GCE/bCNT–dsDNA. Frequency range: 0.1 MHz to 0.1 Hz; potential perturbation: 10 mV; working potential: 0.200 V; redox indicator: 2.0×10^{-3} M [Fe(CN)$_6$]$^{3-/4-}$. The inset shows a zoom of the impedance spectra of GCE, GCE/bCNT and GCE/bCNT–dsDNA. Other conditions are as in (A).
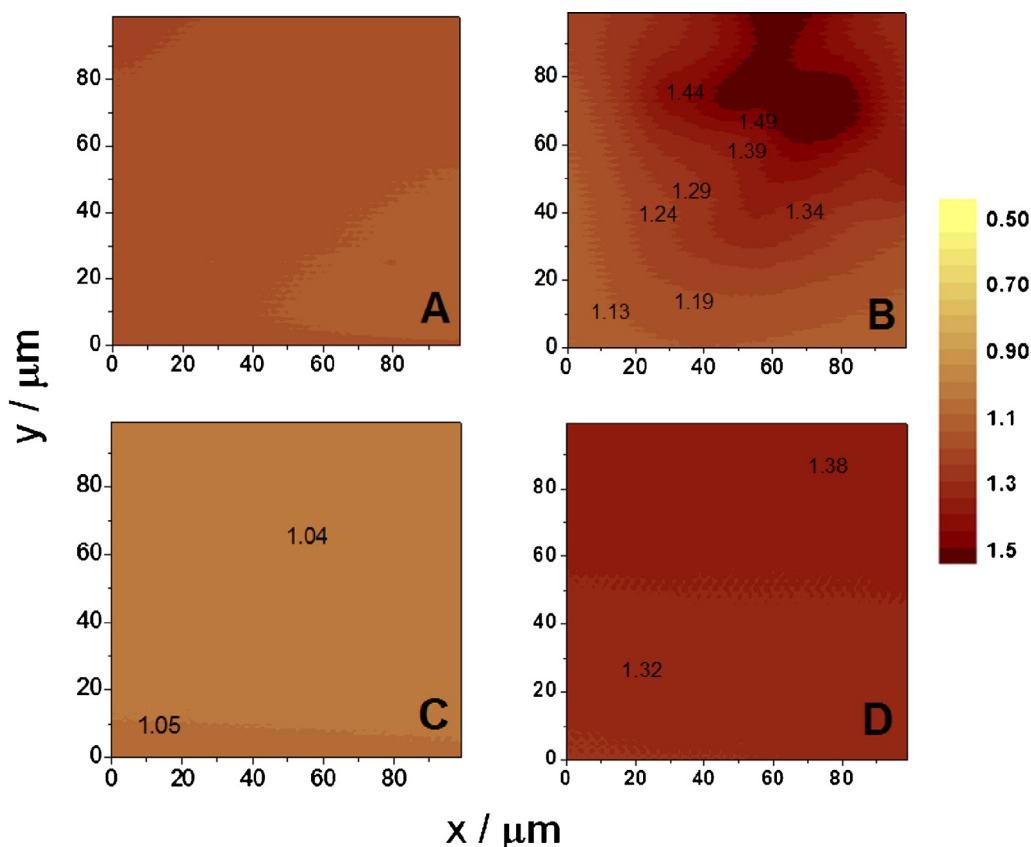
Fig. 4. SECM surface-plots images of (A) bare GCE, (B) GCE/bCNT, (C) GCE/dsDNA and (D) GCE/bCNT–dsDNA. Numbers on the image correspond to the normalized current values. Experimental conditions: 5.0×10^{-4} M FcOH, supporting electrolyte: 0.050 M phosphate buffer solution pH 7.40, $E_T = 0.500$ V, $E_S = 0.000$ V, tip scan rate: $10\,\mu m\,s^{-1}$.

area and the better conductivity of the surface. The adsorption of dsDNA at GCE (C) produces a decrease in the normalized current compared to GCE. This behavior is compatible with a negative feedback between the tip and the substrate, indicating that dsDNA partially blocks the charge transfer of FcOH as it was also demonstrated by EIS and CV experiments. It should be noticed that, since FcOH has no net charge and the oxidation product is $FcO^{\bullet+}$, the decrease in the current is primarily related to a blocking effect. On the contrary, when the dispersion of bCNT in dsDNA solution is deposited at GCE (D), the electroactivity of the surface is homogeneous. The normalized current is slightly smaller than that for GCE/bCNT (in agreement with the EIS results), although it is higher than the one for GCE/dsDNA implying that the nanotubes are efficiently dispersed by the polymer and cover the electrode surface, counteracting the blocking effect of dsDNA.

3.3. Spectroscopic study of bCNT–dsDNA

FTIR spectroscopy it is a very useful technique to evaluate the interaction of polymers with CNT. Fig. 5 shows the FTIR spectra for native dsDNA (a) and bCNT–dsDNA (b). The spectrum for a mixture of 100 ppm dsDNA solution prepared in ethanol:water 50% (v/v) and $1.00\,mg\,mL^{-1}$ bCNT previously sonicated separately for 45 min (c) is also included for comparison. It is important to mention that there are two distinctive spectral regions to get information about the DNA structure: (I) $1800–1500\,cm^{-1}$ region that corresponds to the *in-plane* vibrations of the nitrogen bases and is sensitive to effects of the base pairing and base stacking and (II) $1250–1000\,cm^{-1}$ region that corresponds to sugar–phosphate vibrations and is sensitive to the backbone conformation [50].

The peaks at $1688\,cm^{-1}$ and $1647\,cm^{-1}$ in the dsDNA spectra (a) correspond to the C6=O6 vibration of guanine and the *in-plane* ring vibration of thymine, respectively, and are consistent with a base-paired structure of the DNA. In the spectrum corresponding to bCNT–dsDNA (b) the peak at $1688\,cm^{-1}$ is not evident. There is one peak at $1647\,cm^{-1}$ (corresponding to a double strand conformation) and a new one at $1583\,cm^{-1}$ assigned to the C=N ring vibration of guanine. This last band corresponds to the vibration of unpaired
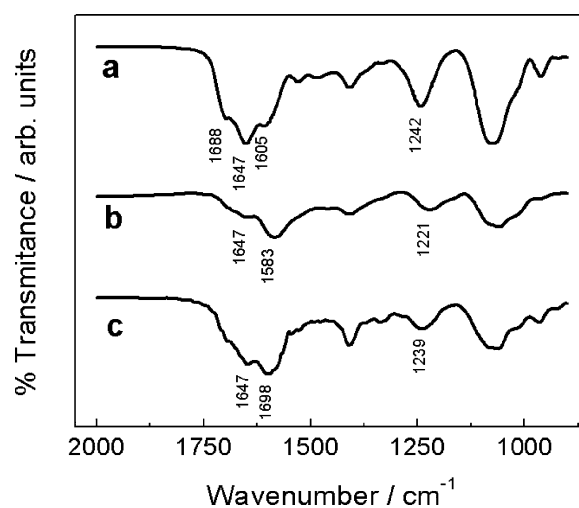

Fig. 5. FTIR spectra for (a) dsDNA, (b) dispersion of bCNT ($1.00\,mg\,mL^{-1}$)–dsDNA (100 ppm) in 50% (v/v) ethanol:water and sonicated for 45 min, and (c) physical mixture of a solution of 100 ppm dsDNA and $1.00\,mg\,mL^{-1}$ bCNT (both prepared in a 50% (v/v) ethanol:water solution) sonicated separately for 45 min and then mixed.
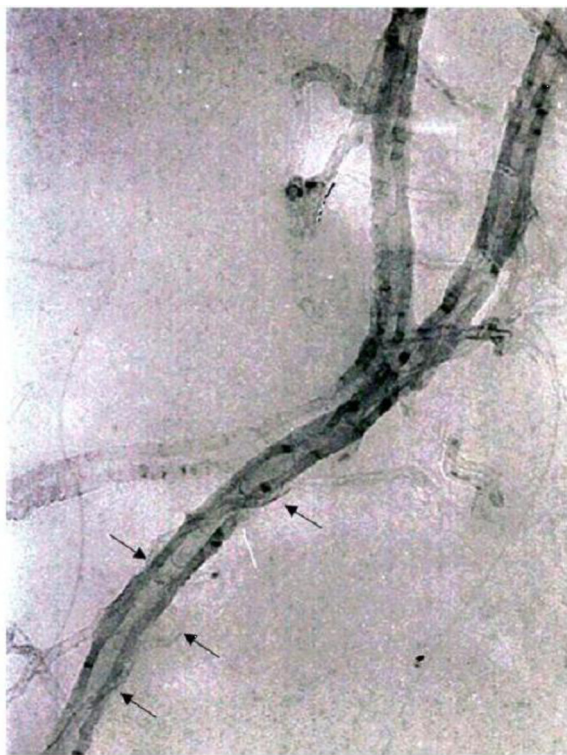
Fig. 6. TEM image of dsDNA dispersing an individual bCNT. The black arrows indicate the wrapping of the bCNT by dsDNA.

guanine and demonstrates that when DNA disperses the bCNT there is a denaturation of the double helix upon the interaction of the bases with the nanotubes sidewalls. However, is important to mention that although the interaction takes place between the unpaired bases and the surface of the nanotubes, there are regions of the DNA which remain in the double stranded form, as it can be seen in the spectrum (b) in the region between 1220 and 1240 cm^{-1}. These bands correspond to the antisymmetric PO_2^- stretching and are characteristic markers of the double stranded conformation (*A*-, *B*- or *Z* forms). These results suggest that the wrapping of DNA around the bCNT present regions of unpaired bases (which interact with the sidewalls) and zones where the double helix structure is preserved.

The spectrum of the physical mixture (c) shows a peak at 1647 cm^{-1} which corresponds to the vibration of the paired thymine as in the previous cases. The vibration of the C=N ring of guanine appears at higher wavenumbers than in the spectrum (b) (1698 cm^{-1}) while the region of the spectrum between 1220 and 1240 cm^{-1} remains similar to the spectra (a) and (b). These results indicate that when the physical mixture between bCNT and dsDNA takes place, the degree of denaturation of dsDNA is lower than in the ultrasonication-assisted dispersion.

The ultrasound-assisted dispersion of bCNT with dsDNA and the presence of ethanol generate important changes in the polymer structure due to the π–π stacking between the bases and the sidewalls of the nanotubes. As the aggregates of nanotubes are exfoliated by the ultrasound cavitation process, the DNA adsorbs through the bases to the sidewalls leaving its hydrophilic backbone exposed to the solution. This non-covalent interaction between aromatic rings was already stated as the driving force of the dispersion of hCNT with DNA, as it reduces the contact area between the polar media and the hydrophobic walls of the nanotubes [51–53]. This wrapping effect is demonstrated in the TEM image depicted in Fig. 6 (indicated by arrows). It is probable that the denatured zones are those in intimate contact with the bCNT while the portions

Table 1

Comparison of the absorbance at 260 nm (A_{260}) and maximum absorption wavelength (λ_{max}) for 100 ppm dsDNA solutions prepared in different media and treated under different conditions.

Solution	Solvent	A_{260}	λ_{max} (nm)
dsDNA	Water	0.202	257.5
dsDNA	50% (v/v) ethanol:water	0.236	260.0
Denatured dsDNA[a]	Water	0.335	260.0
15 min sonicated dsDNA	50% (v/v) ethanol:water	0.256	260.5
30 min sonicated dsDNA	50% (v/v) ethanol:water	0.266	260.5
45 min sonicated	50% (v/v) ethanol:water	0.274	260.5

[a] dsDNA denaturation was carried out by heating the solution in a boiling water bath over 10 min and quickly immersing it in an ice-water bath.

of the double strand which are far from the surface of the nanotube, correspond to a less denatured dsDNA, in agreement with the results reported by other authors for DNA–hCNT interaction [54,55].

3.4. Study of the factors that influence the dispersion of bCNT by dsDNA

3.4.1. Effect of the amount of bCNT

Table S2 (displayed in Supplementary Information) shows the variation of the peak current for guanine electro-oxidation at GCE modified with bCNT–dsDNA dispersions obtained with different amounts of bCNT and 100 ppm dsDNA. The highest peak current for the guanine oxidation is observed using 1.00 mg mL^{-1} bCNT. The incorporation of larger amounts of bCNT in the dispersion do not increase the oxidation current, demonstrating a limited capability of the dsDNA to disperse the CNT. In addition, the non-dispersed bCNT form irregular aggregates that increase the roughness and the real area of the electrode, increasing, consequently, the base line currents and making poor the definition of the guanine oxidation peak.

3.4.2. Effect of the solvent and sonication time

Fig. 7A shows a SEM micrograph of GCE modified with bCNT–dsDNA prepared by mixing 1.00 mg mL^{-1} bCNT with 100 ppm dsDNA (prepared in water) and sonicated for 45 min. The dispersion covers the whole surface; however, even when it is completely covered, it is possible to distinguish a large number of agglomerated bCNT. Fig. 7B displays the SEM micrograph of a GCE modified with bCNT–dsDNA obtained using 50% (v/v) ethanol:water instead of water. The dispersion also covers the whole surface, although, at variance with the previous micrograph, the amount of bCNT bundles drastically decreases, showing that the dispersion of dsDNA is more efficient when using ethanol:water as solvent, as it was observed by SECM images. Fig. 7C depicts one small area of the surface showed in Fig. 7B using higher magnification. In this case is possible to see more clearly the bCNT deposited on the electrode surface. It is important to remark that even when a small zone of the modified GCE disks is shown in the micrograph, the analysis of different areas as well as different samples gave analogous results.

In order to gain further insights about the effect of the solvent and sonication on the dsDNA structure and, in this way to know the incidence of these parameters on the efficiency of the dispersion of bCNT with dsDNA, we performed UV–vis experiments. As it is widely known, the transition between ds and ssDNA can be followed from the increase in the absorbance at 260 nm. Table 1 summarizes the wavelengths for maximum absorption and the absorbances at 260 nm for native dsDNA (dissolved in water) and dsDNA dissolved in ethanol:water (50% (v/v)) after sonicating for different times. For comparison, the information for thermally denatured DNA (dissolved in water) is also included.
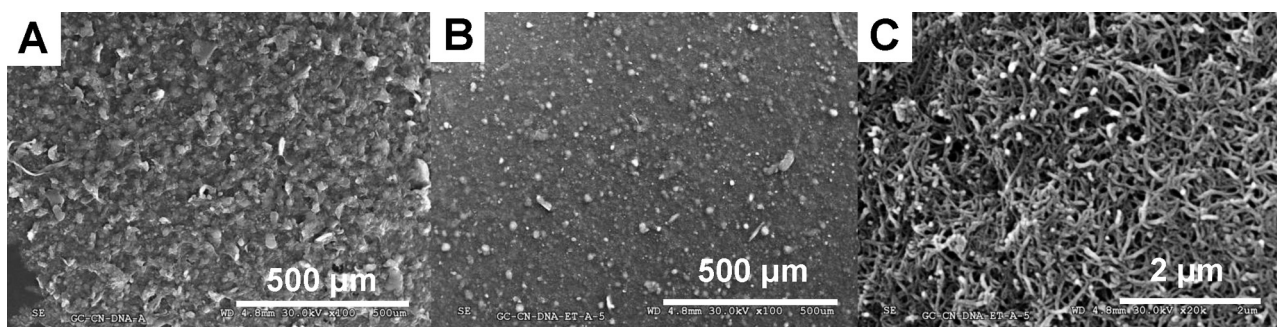
Fig. 7. SEM micrographs of glassy carbon disks modified with dispersions of 1.00 mg mL^{-1} bCNT in a 100 ppm solution of dsDNA using (A) water, (B) and (C) a mixture of 50% (v/v) ethanol:water as solvent, after 45 min sonication. The white bars correspond to the scale: (A and B) 500 μm (100× magnification), (C) 2 μm (20,000× magnification).

The absorbance at 260 nm increases when the dsDNA is dissolved in ethanol:water, and this increase is more pronounced as the sonication time increases. This hyperchromicity suggests a partial denaturation of the DNA.

We also evaluate the influence of the sonication time during the preparation of the dispersion of bCNT with dsDNA in 50% (v/v) ethanol:water from the guanine oxidation signal of the resulting modified GCE (Fig. S6 in Supplementary Information). The guanine oxidation signal increases with the sonication time indicating that the ultrasound treatment in the ethanolic medium produces a change in the biopolymer structure that facilitates the exposure of nucleic acid bases and, in this way, the charge transfer of guanine residues. Another important aspect to consider about the ultrasound treatment is the effect on the size of the dsDNA. Electrophoresis in agarose-gel experiments demonstrated that after 45 min sonication of 100 ppm dsDNA (ca 20,000 base pairs (bp)), the dsDNA is cut in fragments between 200 and 500 bp (not shown). Similar results have been reported for the ultrasound treatment of salmon sperm nuclei DNA [56].

The hyperchromicity and the enhancement in the guanine oxidation signal indicate that the association of the ethanolic medium and the ultrasound facilitates the interaction of the polymer with the sidewalls of the bCNT due to a partial denaturation and a decrease in the length of dsDNA, making possible a more efficient dispersion even when the viscosity of the solvent decreases [16].

4. Conclusions

We report for the first time the successful dispersion of bCNT in dsDNA. Spectroscopic experiments demonstrated that the drastic treatment for dispersing the bCNT (45 min sonication in a 50% (v/v) ethanol:water solution), produces a partial denaturation and a decrease in the length of the dsDNA, that facilitates the dispersion of CNT and makes possible an efficient electron transfer of guanine residues to the electrode. The advantages of modifying GCE with bCNT–dsDNA instead of hCNT–dsDNA on the electron transfer of redox probes and guanine residues are clearly demonstrated. It is important to remark that the resulting GCE/bCNT–dsDNA represents a new alternative to build supramolecular architectures for biosensing, opening the doors to new and exciting possibilities for the development of biosensors using different biorecognition molecules.

Acknowledgements

Appendix A. Supplementary data

Supplementary data associated with this article can be found, in the online version, at http://dx.doi.org/10.1016/j.colsurfb.2013.02.028.

References

[1] K. Balasubramaman, T. Kurkina, A. Ahmad, M. Burghard, K. Kern, J. Mater. Res. 27 (2012) 391.
[2] J.M. Schnorr, T.M. Wager, Chem. Mater. 23 (2011) 646.
[3] A. Jorio, M.S. Dresselhaus, G. Dresselhaus, Topics in Applied Physics, vol. 111, Carbon Nanotubes, Advanced Topics in the Synthesis, Structure, Properties, and Applications, Springer-Verlag, Berlin-Heideberg, 2008.
[4] K.E. Moore, B.S. Flavel, A.V. Ellis, J.G. Shapter, Carbon 49 (2011) 2639.
[5] D. Tasis, N. Tagmatarchis, A. Bianco, M. Prato, Chem. Rev. 106 (2006) 1105.
[6] N. Jia, L. Wang, L. Liu, Q. Zhou, Z. Jiang, Electrochem. Commun. 7 (2005) 349.
[7] L.Y. Heng, A. Chou, J. Yu, Y. Chen, J.J. Gooding, Electrochem. Commun. 7 (2005) 1457.
[8] S. Shanmugann, A. Gedanken, Electrochem. Commun. 8 (2006) 1099.
[9] S. Shanmugann, A. Gedanken, J. Phys. Chem. B 110 (2006) 2037.
[10] S.W. Kim, T. Kim, Y.S. Kim, H.S. Choi, H.J. Lim, S.J. Yang, C.R. Park, Carbon 50 (2012) 3.
[11] C. Gao, Z. Guo, J-H. Liu, X.-J. Huang, Nanoscale 4 (2012) 1948.
[12] L. Hu, D.S. Hecht, G.G. Grüner, Chem. Rev. 110 (2010) 5790.
[13] D. Tuncel, Nanoscale 3 (2011) 3545.
[14] H. Qi, C. Ling, R. Huang, X. Qiu, L. Shangguan, Q. Gao, C. Zhang, Electrochim. Acta 63 (2012) 76.
[15] S. Daniel, T.P. Rao, K.S. Rao, S.U. Rani, G.R.K. Naidu, H.-Y. Lee, T. Kawai, Sens. Actuators B 122 (2007) 672.
[16] Q. Chen, S. Debnath, E. Gregan, H.J. Byrne, J. Phys. Chem. C 114 (2010) 8821.
[17] I. Capek, Adv. Colloid Interface 150 (2009) 63.
[18] Y.Y. Huang, E.M. Terenjev, Polymer 4 (2012) 275.
[19] G.A. Rivas, S.A. Miscoria, J. Desbrieres, G.D. Barrera, Talanta 71 (2007) 270.
[20] E.D. Belashova, N.A. Melnik, N.D. Pismenskaya, K.A. Shevtsova, A.V. Nebavsky, K.A. Lebedev, V.V. Nikonenko, Electrochim. Acta 59 (2012) 412.
[21] S. Bollo, N. Ferreyra, G.A. Rivas, Electroanalysis 19 (2007) 833.
[22] M.D. Rubianes, G.A. Rivas, Electrochem. Commun. 9 (2007) 480.
[23] A. Sánchez Arribas, E. Bermejo, M. Chicharro, A. Zapardiel, G.L. Luque, N.F. Ferreyra, G.A. Rivas, Anal. Chim. Acta 596 (2007) 183.
[24] M.C. Rodríguez, M.D. Rubianes, G.A. Rivas, J. Nanosci. Nanotechnol. 8 (2008) 6003.
[25] G.L. Luque, N.F. Ferreyra, A. Granero, S. Bollo, G.A. Rivas, Electrochim. Acta 56 (2011) 9121.
[26] Y. Jalit, M.C. Rodríguez, M.D. Rubianes, S. Bollo, G.A. Rivas, Electroanalysis 20 (2008) 1623.
[27] M.C. Rodríguez, J. Sandoval, L. Galicia, S. Gutiérrez, G.A. Rivas, Sens. Actuators B 134 (2008) 559.
[28] S. Wang, D. Yu, L. Dai, J. Am. Chem. Soc. 133 (2011) 5182.
[29] A. Liu, I. Honma, M. Ichihara, H. Zhon, Nanotechnology 17 (2006) 2845.
[30] F. Gutiérrez, G. Ortega, J.L. Cabrera, M.D. Rubianes, G.A. Rivas, Electroanalysis 22 (2010) 2650.
[31] J. Filip, J. Sefcovicová, P. Tomcik, P. Gemeiner, J. Tkac, Talanta 84 (2011) 355.
[32] M. Tunckol, J. Durand, P. Serp, Carbon 60 (2012) 4303.
[33] F. Bomboi, A. Bonincontro, C. La Mesa, F. Tardani, J. Colloid Interface Sci. 355 (2011) 342.
[34] F. Gutierrez, M.D. Rubianes, G.A. Rivas, Sens. Actuators B 161 (2012) 191.
[35] V. Sanz, E. Borowiak, P. Lukanov, A.M. Galibert, E. Plahaut, H.M. Coley, S. Ravi, P. Silva, J. Mc Falden, Carbon 49 (2011) 1775.
[36] P. Dalmasso, M.L. Pedano, G.A. Rivas, Anal. Chim. Acta 710 (2012) 58.
[37] B.C. Thompson, S.E. Moulton, K.J. Gilmore, M.J. Higins, P.G. Whitten, G.G. Wallace, Carbon 47 (2009) 1282.

[38] V.A. Karachevtsev, G.O. Gladchenko, M.V. Karachevsev, V.A. Valeev, V.S. Leontiev, O.S. Lytvyn, ChemPhysChem 9 (2008) 2010.
[39] Y. Yamamoto, T. Fujigaya, Y. Niidomea, N. Nakashima, Nanoscale 2 (2010) 1767.
[40] Z. Li, Z. Wu, K. Li, Anal. Biochem. 387 (2009) 267.
[41] J.H. Kim, M. Kataoka, D. Shimamoto, H. Muramatsu, Y.C. Jung, T. Tojo, T. Hayashi, Y.A. Kim, M. Endo, M. Terrones, M.S. Dresselhaus, ChemPhysChem 10 (2009) 2414.
[42] J.M. Hughes, H. Cathcart, J.N. Coleman, J. Phys. Chem. C 114 (2010) 11741.
[43] M.L. Pedano, G.A. Rivas, Biosens. Bioelectron. 18 (2003) 269.
[44] Q. Li, C. Batchelor-McAuley, R.G. Compton, J. Phys. Chem. B 114 (2010) 7423.
[45] C. Wang, G. Zhou, H. Liu, J. Wu, Y. Qiu, B.L. Gu, W. Duan, J. Phys. Chem. B 110 (2006) 10266.
[46] G.L. Luque, M.I. Rojas, G.A. Rivas, E.P.M. Leiva, Electrochim. Acta 56 (2010) 523.
[47] A. Bonanni, M. del Valle, Anal. Chim. Acta 678 (2010) 7.
[48] J.R. Macdonald, J.B. Johnson, Fundamentals of Impedance Spectroscopy, in: E. Barsoukov, J.R. Macdonald (Eds.), Impedance Spectroscopy. Theory, Experiment and Applications, New York, Wiley, 2005.
[49] L.M. Peter, W. Dürr, P. Bindra, H. Gerischer, J. Electroanal. Chem. 71 (1976) 31.
[50] M. Banyay, M. Sarkar, A. Gräslund, Biophys. Chem. 104 (2003) 477.
[51] M. Zheng, A. Jagota, E.D. Semke, B.A. Diner, R.S. McLean, S.R. Lustig, R.E. Richardson, Nat. Mater. 2 (2003) 338.
[52] H. Gao, Y. Kong, Annu. Rev. Mater. Res. 34 (2004) 123.
[53] D. Roxbury, J. Mittal, A. Jagota, Nano Lett. 12 (2012) 1464.
[54] G.O. Gladchenko, M.V. Karachevtsev, V.A. Valeev, V.S. Leontiev, A.Y. Glamazda, A.M. Plokhotnichenko, S.G. Stepanian, Mol. Phys. 104 (2006) 3193.
[55] V.A. Karachevtsev, G.O. Gladchenko, M.V. Karachevtsev, V.A. Valeev, V.S. Leontiev, O.S. Lytvyn, ChemPhysChem 9 (2008) 2010.
[56] T.L. Mann, U.J. Krull, Biosens. Bioelectron. 20 (2004) 945.